Article

# Investigating the Inhibitory Properties of *Cupressus sempervirens* Extract against Copper Corrosion in 0.5 M H$_2$SO$_4$: Combining Quantum (Density Functional Theory Calculation−Monte Carlo Simulation) and Electrochemical-Surface Studies

Khadija Dahmani, Mouhsine Galai,* Adil Ech-Chebab, Nabil Al-Zaqri, Moussa Ouakki, Amr Elgendy, Rabab Ez-Zriouli, Seong-Cheol Kim, Mohamed Ebn Touhami, and Mohammed Cherkaoui

Read Online

ACCESS | 📊 Metrics & More | 📖 Article Recommendations

**ABSTRACT:** The study investigates the potential of *Cupressus sempervirens* (EO) as a sustainable and eco-friendly inhibitor of copper corrosion in a 0.5 M sulfuric acid medium. The electrochemical impedance spectroscopy analysis shows that the effectiveness of corrosion inhibition rises with increasing inhibitor concentrations, reaching 94% with the application of 2 g/L of EO, and potentiodynamic polarization (PDP) studies reveal that EO functions as a mixed-type corrosion inhibitor. In addition, the Langmuir adsorption isotherm is an effective descriptor of its adsorption. Scanning electron microscopy/ energy-dispersive X-ray spectroscopy, atomic force microscopy surface examination, and contact angle measurement indicate that EO may form a barrier layer on the metal surface. Density functional theory calculations, Monte Carlo simulation models, and the radial distribution function were also used to provide a more detailed understanding of the corrosion protection mechanism. Overall, the findings suggest that *Cupressus sempervirens* (EO) has the potential to serve as an effective and sustainable corrosion inhibitor for copper in a sulfuric acid medium, contributing to the development of green corrosion inhibitors for environmentally friendly industrial processes.
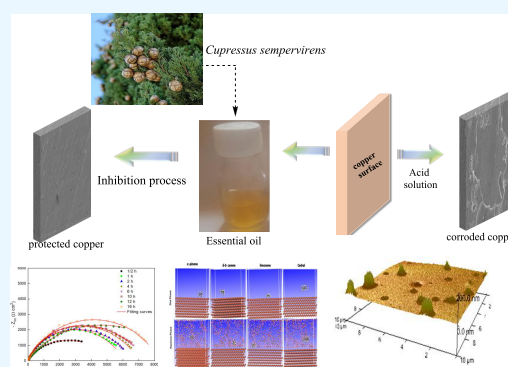
## 1. INTRODUCTION

Cu or alloys are widely employed in various applications because of their great electrical conductivity and thermal as well as good resistance to mechanical effects.[1] It is widely known that copper has a high resistance to atmospheric and chemical attacks due to the development of a protective film on its surface. However, because of the high levels of chloride ions during the acid cleaning and descaling process, copper is very susceptible to corrosion.[2] It is necessary to employ an inhibitor to suppress the Cu corrosion. The use of inhibitors to protect metals and alloys from corrosion under harsh conditions is widely acknowledged. In fact, there have been noteworthy developments in the field of corrosion inhibition in recent years, as shown by several recent publications. These include studies such as refs 3−9. These studies have contributed to our understanding of the mechanisms and properties of various corrosion inhibitors and have demonstrated promising results for their practical applications.

Several organic species have been investigated for corrosion inhibition potential.[10] Based on these studies, organic compounds, especially those containing aromatic structure, N, S, and O functional groups, demonstrated a tremendous

effectiveness in inhibition.[11] A study of the anticorrosive behavior of 5-benzyl-1*H*-tetrazole and 5-(benzylthio)-1*H*-tetrazole on Cu in acidic solution by Qiang et al. showed that its anticorrosive effect mainly depends on the formation of a protective film of self-assembled molecules on the Cu surface.[12] El Hamdani, et al.[13] studied the nature of the inhibiting-corrosion of essential oil (EO) on acidic medium solution. The results from the tests revealed that an anticorrosion benefit was achieved at 94.4% and that this effect was increased as the temperature increased. Zhang et al.[2] examined the effect of corrosion inhibitor anetholitrithionum (ATT) on Cu from acidic solutions of H$_2$SO$_4$. Both experimental and theoretical results revealed that the ATT was an effective anticorrosion inhibitor. The copper corrosion inhibition by Citrus reticulate leaf extract in 0.5 M H$_2$SO$_4$ acid was studied by Xiang et al.[14] It

© 2023 The Authors. Published by American Chemical Society
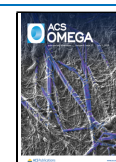
was found that a corrosion inhibition efficiency exceeding 97% can be achieved for an extract concentrate of 500 mg/L.

In addition to the experimental studies, both density functional theory (DFT) and molecular dynamics Monte Carlo (MC) simulation became efficient methods to examine the interrelations between the molecular structure and effectiveness of the inhibition, for finding the optimal adsorption configuration, and for investigating the preferential adsorption sites of organic substances on metal surfaces.[2,15,16]

The use of plant extracts as a green corrosion inhibitor has been widely reported by several authors.[17−22] As an example, Table 1 reports the percentage inhibition efficiency for some

**Table 1. Percentage Inhibition Efficiency for Plant Extracts as a Green Corrosion Inhibitor in Acidic Medium**

| plant extract inhibitor | corrosion inhibition efficiency (%) | medium | reference |
|---|---|---|---|
| *Cupressus sempervirens* | 94.1 | sulfuric | this work |
| *Punica granatum* | 90.0 | hydrochloric acid | 17 |
| *Allium sativum* | 86.3 | | 18 |
| *Zingiber officinale* | 83.2 | | 19 |
| *Emblica officinalis* | 80.7 | | 20 |
| *Azadirachta indica* | 77.6 | | 21 |
| *Syzygium aromaticum* | 74.3 | | 22 |

selected plant extracts used as corrosion inhibitors in acidic medium. By comparing these data, we can show that our inhibitor exhibits better inhibition performance. Furthermore, the novelty of this work lies in the utilization of *Cupressus sempervirens* plant extracts, which are known to be one of the most popular green corrosion inhibitors due to their ease of preparation, versatility in material application, and their minimal harm to both people and the environment.

This paper aims to investigate the new EO inhibitory properties for Cu in 0.5 M $H_2SO_4$ medium, by employing the potentiodynamic polarization plots, the electrochemical impedance spectroscopy (EIS) measurements. The submerged surface of copper has been identified by SEM/EDS, atomic force microscopy (AFM) spectroscopy, and contact angle measurements. The experimental investigation was validated through the use of both quantum chemical analysis and molecular dynamics simulations to evaluate the material properties.

The objective of this research paper is to investigate the inhibitory properties of a new EO on copper in a 0.5 M $H_2SO_4$ medium. To achieve this goal, a range of techniques were employed, including potentiodynamic polarization plots, EIS measurements, and SEM/EDS, AFM spectroscopy, and, contact angle measurements to identify the submerged surface of copper. The validity of the experimental results was confirmed using quantum chemical analysis and molecular dynamics simulations to assess the material properties.

## 2. EXPERIMENTAL PART

**2.1. Isolation of the EO.** Samples of *C. sempervirens* were obtained from the Western High Atlas of Morocco (Aghbar forest). Before extraction, the leaves were dried in the shade in a ventilated area. The EO was extracted by hydro distillation using a Clevenger type apparatus, and 250 g of dried leaves of *C. sempervirens* are put in contact with distilled water in a container for three hours at 100 °C. The oil obtained is then dehydrated

with anhydrous sodium sulfate and stored at 4 °C in the shade for future use.

**2.2. Analysis of the EO by GC/MS.** In order to determine the chemical composition of the EO obtained, an analysis by chromatography coupled to a mass spectrum (GC/MS) has been performed using a Thermo Fischer capillary gas chromatograph directly coupled to a mass spectrometry system (model GC ULTRAS/N 210729).[23]

**2.3. Compound, Material, and Its Preparation.** The copper used in this research is commercial grade with the following chemical composition (in wt %): 0.019 P, <0.001 Fe, <0.001 As, <0.001 Mn, <0.002Sb, <0.001 Al, 0.009 Sn, 0.003 Ni, 0.015 Pb, <0.005 Ag, <0.001 Bi, <0.001 S, <0.005 C, and the balance being Cu. Coupons with dimensions of 2.5 cm × 2.0 cm × 0.05 cm were used for electrochemical measurements after being abraded with various abrasive paper qualities and thoroughly cleaned with acetone and distilled water before being placed on a hot air dryer.[24] The testing solutions were prepared using analytical-grade reagents and 98% $H_2SO_4$ distilled water.

**2.4. Electrochemistry Measurements.** The electrochemical measurements were conducted using a PGZ100 potentiostat controlled by the Volta Master software and connected to three electrodes: a reference electrode (SCE), an auxiliary platinum electrode, and a copper work electrode with a 1 cm² exposure area. Electrochemical calculations were performed for two hours at 298 K after immersion. The polarization was recorded at a scan rate of 1 mV/s over a potential range of −600 to +600 mV/SCE, with a 10 min interval between experiments for the formation and stabilization of the electric double layer. The electrochemical impedance measurements were performed over a frequency range of 100 kHz to 10 mHz with 10 mV signal amplitude.

**2.5. MEB/EDS Analysis.** SEM/EDS analysis (JOEL JSM-5500) has been applied for the surface and chemical morphology, respectively. This copper characterization in 0.5 M $H_2SO_4$ without and with EO was conducted following 6 h of immersion.

**2.6. Computational Chemical Studies.** Material Studio version 6.0 from Accelrys was employed to perform the quantum calculations of the constituent compounds of the EO. The compounds were geometry optimized to the fundamental state using the DMol3 module and DND basis set. Many DFT reactivity parameters have been determined. This includes the energy of the molecular boundary orbitals ($E_{HOMO}$ and $E_{LUMO}$). Based on the following equations, the energy gap ($\Delta E$), hardness ($\eta$), softness ($\sigma$), electronegativity ($\chi$), and number of transferred electrons ($\Delta N$) can be obtained.[25]

The energy gap $\Delta E$ is given by

$$\Delta E = E_{LUMO} - E_{HOMO} \tag{1}$$

where $E_{HOMO}$ denotes the energy of the highest occupied molecular orbital and $E_{LUMO}$ is the lowest unoccupied molecular orbital energy.

The electronegativity $\chi$, which shows the ability of atom to draw electrons, the global chemical hardness $\eta$, which indicates the resistance of the atom to charge transfer, and the global chemical softness $\sigma$, which is a commonly utilized reactivity parameter, are calculated as:

$$\chi = \frac{I + A}{2} \tag{2}$$

$$\eta = \frac{I - A}{2} \qquad \sigma = \frac{1}{\eta} \qquad (3)$$

where $A$ is the electron affinity and $I$ is the ionization potential. The fraction of transferred electrons ($\Delta N$) is reported as:

$$\Delta N = \frac{\Phi_{Cu} - \chi_{inh}}{2(\eta_{Cu} + \eta_{inh})} \qquad (4)$$

where $\Phi_{Cu}$, $\chi_{inh}$, $\eta_{Cu}$, and $\eta_{inh}$ represent, respectively, the work function of copper, the inhibitor's electronegativity, and the hardnesses of copper and the inhibitor. The $\Phi_{Cu}$ and $\eta_{Cu}$ values for Cu(111) are taken as 4.80 eV and 0.0 eV/mol, respectively.[26]

Using a combination of all previously mentioned parameters, the inhibition capabilities of the compounds can be understood. Furthermore, using MC simulations, the interaction between the active component and the Cu surface was investigated. The simulations were investigated with adsorption locators in the materials studio package. A simulation cell with a periodic boundary was established in this study on the previously described Cu(111) surfaces with similar conditions.[25] where a vacuum layer (25 Å³ vacuum) was filled with the chemical species ($\alpha$-Pinene, $\delta$-3-Carene, Limonene, and Cedrol). The adsorption of the active compounds over the most representative Cu(111) plane was carried out in the gas and solvent phase with a view to minimizing the corrosion inhibition effects. In the solvent environment, about 500 water molecules as well as 50 molecules of $H_3O^+$ and $SO_4^{2-}$ have been added to the compounds tested.[26]

## 3. DISCUSSION AND THE RESULTS OF THE STUDY

**3.1. *Cupressus sempervirens* Chemical Composition.** The results of a quantitative analysis by gas chromatography—mass spectrometry of *C. sempervirens* EO showed in Table 2. Fourteen volatile compounds have been identified with retention index and distribution area representing 96.7% in the oil.$\alpha$-pinene (37.07%) has been found as the most abundant compound, followed by the $\alpha$-pinene, $\delta$-3-carene (18.55%) and limonene (12.65%), and cedrol (12.24%). Other chemicals are also available at a medium rate, such as myrcene (4.33%) and D-germacrene (3.99%).

**3.2. Open Circuit Potential (OCP) Measurements.** OCP and its evolution with time in the investigated acidic medium before and after the addition of various concentrations of EO after 0.5 h of immersion at 298 K are displayed in Figure 1. It can be seen that the presence of EO investigated species leads to a slight displacement of $E_{corr}$ to positive and negative potentials compared to the blank solution.

**3.3. EIS Measurements.** Figures 2a−c and 3 show the Nyquist and Bode curves with the corresponding equivalent circuit that fits the EIS experimental data related to the Cu electrode both with and without diverse concentrations of EO in 0.5 M $H_2SO_4$ aerated solution at 303 K, respectively. The resulting impedance diagrams reveal semicircles with flattened capacitance loops. This flattened semicircle is attributed to the dispersion effect.[27−29] In these Nyquist patterns, two poorly differentiated capacitance loops are presented for all concentrations except the concentration which presents two well-defined capacitive loops. One possible reason for the double capacitive loop in the Nyquist plot could be the presence of adsorbed species on the electrode surface. When a molecule adsorbs onto the electrode surface, it creates a capacitance that is different from the double layer capacitance. This can result in a

**Table 2. Chemical Analysis of *Cupressus sempervirens* Essential Oil**

| chemical compounds | retention index (RI) | *C. sempervirens* (%) |
|---|---|---|
| tricyclene | 913 | |
| $\alpha$-thujene | 925 | 0.68 |
| camphene | 933 | |
| $\alpha$-pinene | 937 | 37.07 |
| $\beta$−pinene | 976 | 2.25 |
| myrcene | 989 | 4.33 |
| $\Delta$-3-carene | 1003 | |
| $\delta$-3-carene | 1005 | 18.55 |
| $\alpha$-phellandrene | 1008 | |
| limonene | 1029 | 12.65 |
| 1,8-cineole | 1033 | |
| $\gamma$-terpinene | 1062 | |
| *para*-cymene | 1067 | |
| terpinolene | 1084 | 1.81 |
| linalool | 1098 | |
| $\alpha$-terpineol | 1137 | |
| borneol | 1155 | 0.03 |
| $\alpha$-terpineol | 1171 | 0.22 |
| terpinene-4-ol | 1177 | |
| copaene | 1179 | |
| $\alpha$-terpineol | 1189 | |
| *trans*-cadina-1(6),4-diene | 1224 | |
| carvacrol | 1290 | 0.87 |
| myrtenyl acetate | 1335 | |
| $\beta$-caryophyllene | 1418 | |
| D-germacrene | 1478 | 3.99 |
| $\gamma$-cadinene | 1510 | 0.89 |
| $\delta$-cadinene | 1515 | 1.12 |
| isoeugenol acetate | 1563 | |
| caryophyllene oxide | 1575 | |
| cedrol | 1609 | 12.24 |
| total | | **96.7** |
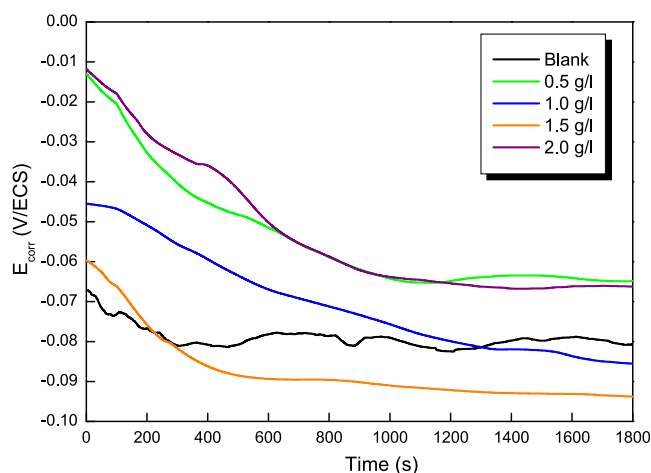


**Figure 1.** OCP and its evolution with time in 0.5 M $H_2SO_4$ medium before and after adding various concentrations of EO at 298 K.

second capacitive loop in the Nyquist plot, indicating the presence of an adsorbed species. Consequently, the first loop at a low frequency is due to the charge transfer resistance and the double layer capacitance, while the other loop at a high frequency is caused by the adsorption of the EO molecules on the copper surface. Moreover, when the EO concentration increases, the diameter of the capacitive loop also rises, reflecting
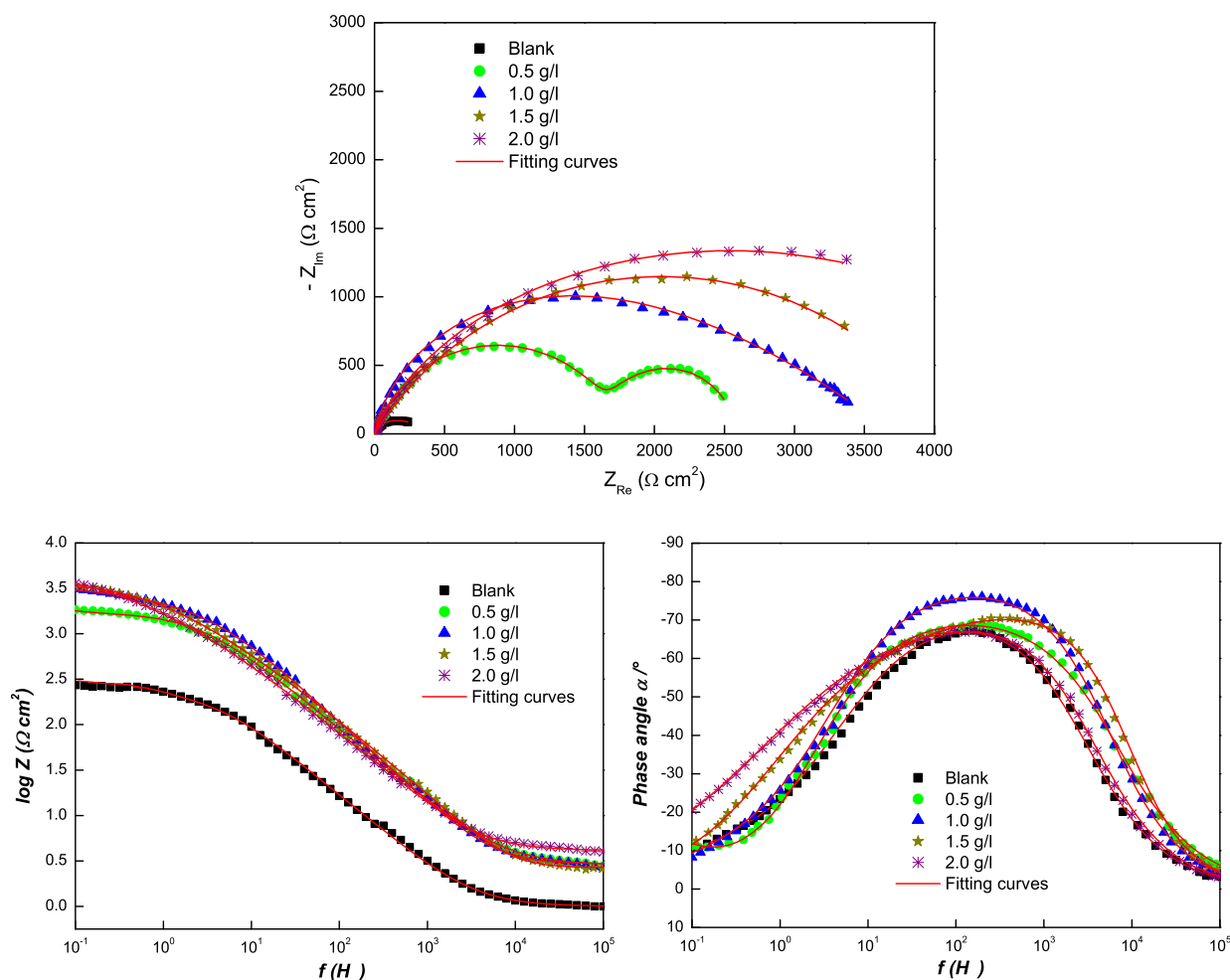
**Figure 2.** Nyquist as well as Bode plots of copper metal in 0.5 M H$_2$SO$_4$ solution at 298 K without and with varying concentrations of essential oil (EO) inhibitor.



**Figure 3.** Fitting EIS data with corresponding circuits.

the inhibitory effects of the EO due to the increasing charge transfer resistance. This is caused by the development of the protective film formed on the copper surface, preventing the development of corrosion.[30]

To interpret these results, we have modeled the impedance diagrams with the electrical circuits displayed in Figure 3 where $R_s$ is referred to the resistance of the solution, $R_f$ is related to the resistance of the oxide layer and the film of the inhibitor on the copper surface, and $R_{ct}$ is assumed to be the charge transfer resistance. The constant phase elements (CPE$_f$) of the oxide film and the double layer are defined as CPE$_f$ and CPE$_{dl}$, respectively.[30]

Nevertheless, the use of the CPE in fitting Nyquist curves has been related to the inhomogeneity and other reasons (impurities, adsorption spices) of the Cu surface.[31] The CPE impedance is calculated by eq 5:[32,33]

$$Z_{CPE} = [Q(j\omega)^n]^{-1} \tag{5}$$

where $\omega$ is the angular frequency, j is the imaginary unit, and $n$ is the parameter of deviation related to the phase deviation, which is one of the most important aspects of the CPE. When $n = 0$, the CPE is like a pure resistor; for $n = 1$, the CPE is a pure capacitor.[34]

Inhibitory efficacy (IE) was evaluated using eq 6:[35]

$$IE = \left( \frac{R_p - R_{ct}^{\circ}}{R_p} \right) \times 100\% \tag{6}$$

where $R_{ct}$ and $R_{ct}^{\circ}$ represent the charge transfer resistance in inhibited and uninhibited conditions, respectively.[36] The electrochemical data derived by simulating their impedance plots using the EC-Lab software via equivalent circuit are given in Table 3.

**Table 3. Impendence Parameters of Cu with and without EO in 0.5 M H$_2$SO$_4$**

| medium | [C] (g/L) | $R_s$ (Ω cm²) | $R_f$ (Ω cm²) | $CPE_f$ (μF s$^{n-1}$ cm$^{-2}$) | $n_f$ | $R_{ct}$ (Ω cm²) | $CPE_{dl}$ (μF s$^{n-1}$ cm$^{-2}$) | $n_{dl}$ | $R_p$ (Ω cm²)[a] | $\chi^2$ | $\theta$ | IE (%) |
|---|---|---|---|---|---|---|---|---|---|---|---|---|
| 0.5 M H$_2$SO$_4$ | blank | 0.7 ± 0.1 | | | | 350 ± 2.5 | 475 ± 2.1 | 0.72 ± 0.03 | 350 | 0.07 | | |
| EO | 0.5 | 2.8 ± 0.2 | 1746 ± 2.5 | 59.6 ± 0.9 | 0.81 ± 0.02 | 828 ± 2.7 | 377 ± 2.6 | 0.95 ± 0.05 | 2574 | 0.03 | 0.864 | 86.4 |
| | 1.0 | 2.9 ± 0.4 | 1655 ± 3.6 | 62.3 ± 1.3 | 0.89 ± 0.05 | 2025 ± 3.2 | 39.4 ± 1.3 | 0.91 ± 0.08 | 3680 | 0.04 | 0.905 | 90.5 |
| | 1.5 | 2.5 ± 0.8 | 546 ± 1.8 | 415.2 ± 2.7 | 0.77 ± 0.02 | 3623 ± 3.6 | 28.8 ± 1.0 | 0.88 ± 0.1 | 4169 | 0.06 | 0.916 | 91.6 |
| | 2.0 | 2.6 ± 0.5 | 447 ± 2.0 | 428.8 ± 3.2 | 0.85 ± 0.03 | 5191 ± 4.3 | 13.5 ± 0.8 | 0.87 ± 0.09 | 5638 | 0.02 | 0.938 | 93.8 |

$^a$The $R_p$ is polarization resistance.

From Figure 2, the Bode images reveal that the presence of inhibitor EO leads to a significant increase in phase angle values and impedance modulus at low frequencies, indicating that the inhibitor is able to form a highly effective adsorption layer at the copper/solution interface, which impedes copper corrosion. Moreover, the increase in impedance modulus at low frequencies suggests that the inhibitor layer becomes denser and more efficient with increasing EO concentration. At the highest concentration tested (2 g/L), the log |Z| value is 1.5 orders of magnitude higher than that of the bare copper substrate, demonstrating the strong inhibition performance of EO in an acidic environment. Overall, these results suggest that EO is a potent inhibitor for copper corrosion, and its inhibition effectiveness increases with increasing concentration.[37,38]

From Table 3 data, it appears that as the concentration of EO in the corrosive solution is further increased, the $R_{ct}$ and $R_f$ increase, whereas the $CPE_f$ and $CPE_{dl}$ decrease respectively, demonstrating an increase in the inhibition effectiveness at the same time. This indicates that the molecules of the EOs replace the chloride ions Cl$^-$ on the electrode's surface to create an anticorrosion layer that protects against corrosion attacks.[15]

**3.4. Polarization Measurements.** Polarization measurements have been performed for obtaining corrosive current densities ($i_{corr}$), corrosive potentials ($E_{corr}$), and the cathodic and anodic Tafel slopes ($\beta_a$ and $\beta_c$). Furthermore, the inhibition efficiency (IE) was derived using the following formula:[2,29]

$$IE = \left(1 - \frac{i_{corr}}{i_{corr}^\circ}\right) \times 100\% \tag{7}$$

where $i_{corr}$ and $i_{corr}^\circ$ represent the current corrosion density for the system with and without the inhibitor, respectively. The relevant electrochemical measurements are presented in Table 3. Based on Figure 4 as well as Table 4, there is evidence that the
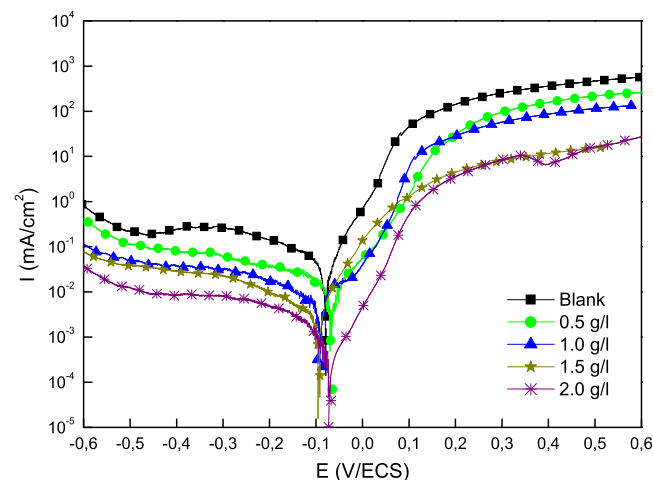


**Figure 4.** Potentiodynamic polarization graphs for Cu in 0.5 M H$_2$SO$_4$ with EO at various concentrations.

addition of EO produces a significant negative shift in the corrosion potential of copper. However, there is less than 85 mV of maximum corrosion potential movement, which leads to the conclusion that the EO acts as a mix corrosion inhibitor[39] and significant decreases in anodic and cathodic current density compared to the blank solution. Moreover, the density of the corrosion current is continuing to reduce, meaning that the anode reaction (Cu dissolution) and cathode reaction (O

**Table 4. Electromechanical Parameters Derived from Potentiodynamic Polarization Plots of Cu in 0.5 M H$_2$SO$_4$ at Various Concentrations of EO at 298 K**

| compounds | [C] (g/L) | $-E_{corr}$ (mV/ECS) | $i_{corr}$ ($\mu$A/cm$^2$) | $-\beta_c$ (mV dec$^{-1}$) | $\beta_a$ (mV dec$^{-1}$) | IE (%) |
|---|---|---|---|---|---|---|
| 0.5 M H$_2$SO$_4$ | blank | 79 | 29.0 | 204 | 59 | |
| EO | 0.5 | 64 | 3.8 | 195 | 57 | 86.9 |
| | 1.0 | 85 | 2.7 | 181 | 54 | 90.7 |
| | 1.5 | 93 | 2.3 | 176 | 52 | 92.0 |
| | 2.0 | 66 | 1.7 | 170 | 49 | 94.1 |

reduction) are being suppressed, especially since the change in the cathode is more apparent. Moreover, the $\beta c$ of the slope of the Tafel curve decreases significantly and differs from blank. Due to the adsorption of various EO molecules on the copper surface, which becomes denser from the accumulation effect and inhibits the active inhibitory sites on the copper electrode surface, the corrosion resistance behavior mostly depends on the lowering of the current density.[40,33] In this work, the compound EO was introduced as an inhibitor of corrosion and was applied to the copper for protection in the sulfuric acid solution for the first time. In order to clarify the anticorrosion mechanism, it is important to understand the interaction between copper and EO. The electrochemical performance and microscopic morphology evidence strongly indicate that the adsorption film is formed on the copper surface under an acidic medium.[36] The results in Figure 3 demonstrate a parallel tendency, which indicates that the mechanism for the cathodic reactions is not modified by the absorption of the inhibiting molecules. The cathodic process mechanism is shown in the following way:[41]

$$\frac{1}{2}O_2 + 2H^+ + 2e^- \rightarrow H_2O \tag{8}$$
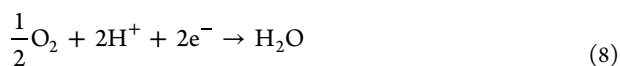
The anode mechanism of reaction is given below:[16]

$$Cu \rightleftarrows Cu^+_{ads} + e^- \quad (fast) \tag{9}$$

$$Cu^+_{ads} \rightleftarrows Cu^{2+} + e^- \quad (slow) \tag{10}$$
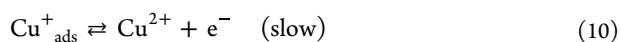
According to the mechanism of the reactions (eqs 9 and 10), we can see that the Cu electrode can generate cuprous ions in sulfuric acid and air solution. Consequently, the inhibiting compound is most likely to coordinate with the cuprous ion so that it adsorbs on the surface of the Cu electrode, and the interaction mechanism is given by:[42]

$$Cu^+_{ads} + nInh \rightarrow [Cu-Inh_n]^+_{ads} \tag{11}$$
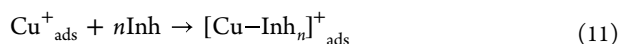
**3.5. Impact of Immersion Time.** Impact of submersion time is investigated at optimum concentration of EO from 0.5 to 16 h, employing measurement of EIS. The Nyquist diagrams as a function of immersion time at 298 K are shown in Figure 5 with their electrochemical parameter listed below in Table 4. We see that the Nyquist plots increase with increasing time of immersion, which suggests that EO exhibits significant inhibition of Cu corrosion in 0.5 M H$_2$SO$_4$. Based on Table 5, it is clear that the $R_{ct}$ value increases with increasing time, while the value of CPE$_{dl}$ decreases. The increasing $R_{ct}$ values may be due to the development of a deterrent layer on the copper interface. The reduction in CPE$_{dl}$ was probably a consequence of an increase in the electronic double layer.

**3.6. Adsorption Isotherm.** The study of adsorption isotherms is crucial to understand the mechanisms of inhibition corrosion reactions. In order to find the most appropriate isotherm model for our inhibitor, we have plotted the various
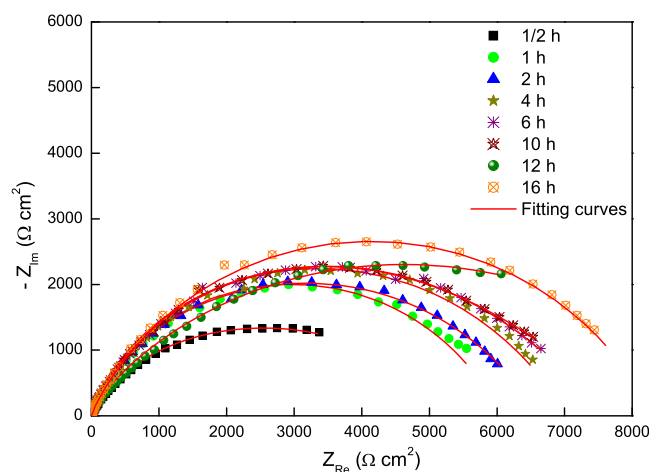
**Figure 5.** Nyquist diagrams for cooper in 0.5 M H$_2$SO$_4$ through various periods of immersion in the presence of EO.

adsorption isotherm models using their mathematical eqs 8−11:[43,44]

$$\text{Langmuir:} \quad \frac{C_{inh}}{\theta} = \frac{1}{K_{ads}} + C_{inh} \tag{12}$$

$$\text{Temkin:} \quad \theta = -\frac{1}{2a}\ln(K_{ads}) - \frac{1}{2a}\ln(C_{inh}) \tag{13}$$

$$\text{Freundlich:} \quad \ln\theta = \ln(K_{ads}) + a\ln(C_{inh}) \tag{14}$$

$$\text{Al-awady:} \quad \ln\left(\frac{\theta}{1-\theta}\right) = \ln(K_{ads}) + y\ln(C_{inh}) \tag{15}$$

in which $\theta$ is the metal surface coverage which is determined by eq 2, $C_{inh}$ is the concentration of EO, $y$ is the parameter of heterogeneity, $a$ is the lateral interaction term, and $K_{ads}$ is the equilibration constant, which is linked to $\Delta G_{ads}$ by eq 16:[45−47]

$$K_{ads} = \frac{1}{1000}\exp\left(-\frac{\Delta G^\circ_{ads}}{RT}\right) \tag{16}$$

where $R$ stands for the gas constant, $T$ stands for temperature, which is equal to 298 K and $C_{H_2O}$ represents the concentration of the water of the solution, equal to 1000 g L$^{-1}$. From Table 6, it is evident that $R^2$ is close to unity for the Langmuir isotherm. From this, we may conclude that Langmuir is the best isotherm.[48] Moreover, from Figure 6, the variation of the relationship between $C_{inh}/\theta$ and $C_{inh}$ is linear with a slope value close to 1 (0.96258),which confirms the validity of the Langmuir isotherm.[32,11]

This isotherm presupposes that the adsorbed species and the metal surface are attracted to or repellent to one another. In addition, a negative value for the slope suggests that interaction is laterally repulsive in the absorbing layer. Furthermore, as a

**Table 5. Electrochemical Impedance Parameters for Cooper in 0.5 M $H_2SO_4$ at Different Concentrations of EO**

| medium | time (h) | $R_s$ ($\Omega$ cm²) | $R_f$ ($\Omega$ cm²) | CPE$_f$ ($\mu$F s$^{n-1}$ cm$^{-2}$) | $n_f$ | $R_{ct}$ ($\Omega$ cm²) | CPE$_{dl}$ ($\mu$F s$^{n-1}$ cm$^{-2}$) | $n_{dl}$ | $R_p$ ($\Omega$ cm²)[a] | $\chi^2$ |
|---|---|---|---|---|---|---|---|---|---|---|
| EO | 0.5 | 2.6 ± 0.5 | 447 ± 2.0 | 428.8 ± 3.2 | 0.85 ± 0.03 | 5191 ± 4.3 | 13.5 ± 0.8 | 0.87 ± 0.09 | 5638 | 0.02 |
|  | 01 | 2.1 ± 0.4 | 116 ± 3.2 | 1131 ± 5.2 | 0.96 ± 0.04 | 5982 ± 5.6 | 12.8 ± 1.0 | 0.74 ± 0.03 | 6098 | 0.04 |
|  | 02 | 2.4 ± 0.6 | 628 ± 2.9 | 372 ± 3.0 | 0.86 ± 0.07 | 6047 ± 4.7 | 11.2 ± 0.9 | 0.69 ± 0.05 | 6675 | 0.03 |
|  | 04 | 2.0 ± 0.3 | 677 ± 2.4 | 358 ± 2.6 | 0.97 ± 0.02 | 6428 ± 3.8 | 10.9 ± 0.6 | 0.68 ± 0.07 | 7105 | 0.07 |
|  | 06 | 1.2 ± 0.1 | 1090 ± 3.0 | 287 ± 1.8 | 0.80 ± 0.07 | 6752 ± 4.3 | 10.1 ± 0.5 | 0.75 ± 0.03 | 7842 | 0.05 |
|  | 10 | 1.3 ± 0.2 | 1521 ± 3.6 | 241 ± 2.1 | 0.79 ± 0.06 | 6784 ± 4.2 | 13.1 ± 1.3 | 0.78 ± 0.04 | 8305 | 0.06 |
|  | 12 | 2.1 ± 0.1 | 606 ± 2.3 | 384 ± 2.5 | 0.96 ± 0.08 | 7864 ± 5.2 | 8.2 ± 0.4 | 0.69 ± 0.06 | 8470 | 0.1 |
|  | 16 | 1.4 ± 0.5 | 766 ± 1.9 | 318 ± 3.0 | 0.73 ± 0.05 | 7920 ± 3.6 | 180 ± 2.0 | 0.88 ± 0.04 | 8686 | 0.04 |

[a]The $R_p$ is polarization resistance.

**Table 6. Corresponding Correlation Coefficients ($R^2$) of the Adsorption Model Isotherms (Langmuir, Temkin, Freundlich, and Al-Awady) of EO**

| adsorption isotherm | $R^2$ |
|---|---|
| Langmuir | **0.99987** |
| Temkin | 0.99079 |
| Freundlich | 0.99075 |
| Al-Awady | 0.99798 |

result, a negative value of $\Delta G_{ads}$ shows that the adsorption processes is spontaneous and the stability of the adsorbed layer on the metal surface is high.[32] In general, higher values of $\Delta G_{ads}$, around −20 kJ mol$^{-1}$ or less, are related to electrostatic properties between charged molecules and the metal (physical adsorption), while values around −40 kJ mol$^{-1}$ and higher represent charge transfer from organic molecules to metallic surface (chemisorption).[49] This would seem to indicate that the inhibiting action of this important compound is the physical adsorption with a tendency to chemisorption (Table 7).

**3.7. SEM/EDS Analysis.** Figures 7 and 8 displays SEM/EDS images of Cu samples submerged in 0.5 M $H_2SO_4$ at 303 K for 24 h with or without 2.0 g L$^{-1}$ EO, and the surface elemental composition is recorded in Table 8. We can clearly see that the
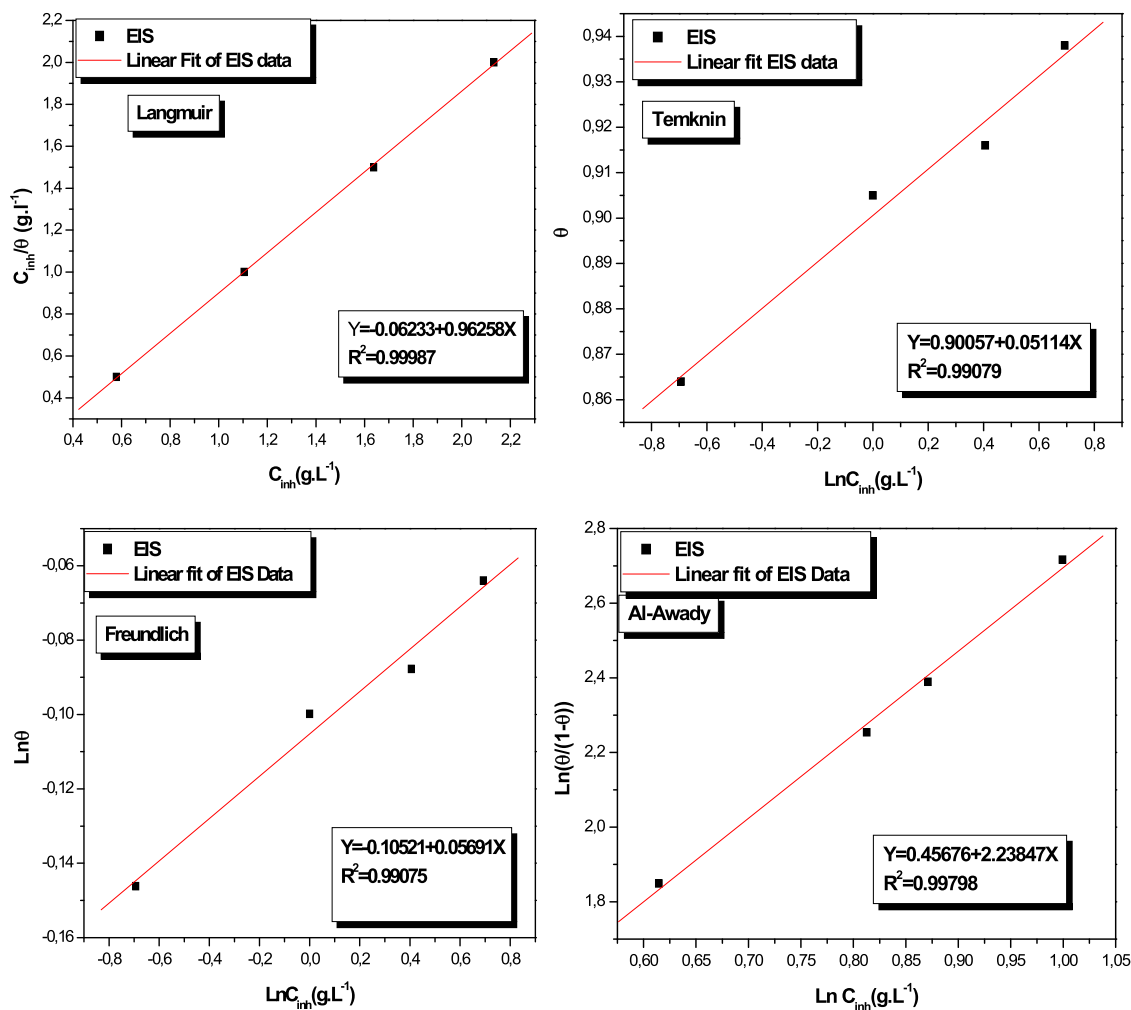


**Figure 6.** Graphs of the different adsorption isotherms of EO for the Cu surface in 0.5 M $H_2SO_4$ at 298 K.

**Table 7. Langmuir Adsorption Isotherms for Values Calculated for EO**

| isotherm | $R^2$ | slope | $K_{ads}$ (L g$^{-1}$) | $\Delta G°_{ads}$ (kJ mol$^{-1}$) |
|---|---|---|---|---|
| Langmuir | 0.99987 | 0.96258 | 16.04 | 24.39 |

surface of copper is strongly corroded. Some corrosion products, some cavities, and some scratches appear on the Cu in 0.5 M $H_2SO_4$ alone. Whereas after adding 2.0 g/L of EO, the surface morphology became smooth and the damaged and corroded parts of the copper surface have been extremely decreased. The pictures show that the passive film has effectively covered the Cu surface and has blocked the active sites. The EDS spectra in the presence of 2.0 g/L EO revealed an additional peak, which was due to nitrogen atom "N" of essential oil that is responsible for copper protection.[11] Furthermore, a high level of "S" linked to sulfuric acid was found on the surface of Cu submerged in acid with no inhibitor, indicating a high attack of the acid. These SEM findings are coherent with electrochemical experimental results.

**3.8. AFM Analysis.** Figure 9 illustrates the 2D and 3D morphology of the Cu samples submerged in 0.5 M $H_2SO_4$ alone and with 2.0 g L$^{-1}$ EO and the related surface roughness (Ra) for 16 h. A ton of dips, peakss, and valleys are seen on the surface of the corroded Cu (Figure 9a) where the roughness reaches 121 nm.[50] On the other hand, in comparison with the copper noncorroded, the surface of copper exhibits a flatter and smoother surface after immersing in a sulfuric acid solution containing EO stable (Figure 9b) and Ra is found to be 4.79 nm. From the results given above, it appears that EO was adsorbed on a Cu surface in a solution of sulfuric acid. It may be attributed to the bigger EO carrying more heterocyclic rings as well as larger carbon chains, which thus conducts stronger chemical coordination with Cu ions.[51]

**3.9. Contact Angle Calculations.** Contact angle calculations results achieved for Cu submerged in 0.5 M $H_2SO_4$ both with and without 2.0 g/L for 16 h are presented in Figure 10. From the results, we can observe that contact angle in the presence of EO has reached 88.3°, and blank has reached 41.5° revealing the hydrophobicity of the surface.[52,53] The adsorption of the EO organic molecules on the Cu active site was responsible for increasing the angle of contact. These results confirmed that organic molecules of EO were capable of adsorbing on the copper and inhibiting it from corrosion.[54] The contact angle measured across the surface of Cu in the blank solution is 41.5°, which indicates that the surface roughness is high and therefore corrosion is progressing.[55]

**3.10. DFT Computations and MC Simulations.** DFT studies have been conducted on the major ingredients of the essential oil, to investigate their inhibition performance toward the Cu metal surface in 0.5 M $H_2SO_4$. The optimized structure of the four considered components ($\alpha$-pinene, $\delta$-3-carene, limonene, and cedral), and their corresponding FMO electronic distribution (HOMO and LUMO) are presented in Figure 11.

The optimized molecular patterns show the most stable configuration of the investigated compounds. We can see that the electron density distribution of FMO has been distributed throughout the $\alpha$-pinene structure, unlike other compounds, which demonstrates that the structure has various electron donor and acceptor moieties.[56] Additionally, the electrostatic potential (ESP) shows the nucleophilic (red) and electrophilic (blue) positions. This indicates that when the EO components adsorbed on the Cu surface then nucleophilic atoms are usually the primary active moieties that adsorbed on the Cu surface protecting it from the ions.[57] Different computed quantum parameters related to the most stable configuration are shown in Table 9. Generally, $E_{HOMO}$ describes a molecule's ability to give electrons to a potential acceptor. On the other hand, $E_{LUMO}$ denotes the capacity of a molecule to accept electrons from a species. On the basis of the difference ($E_{LUMO} - E_{HOMO}$), this defines the energy gap ($\Delta E$). A greater value of $\Delta E$ signifies a smaller chemical reactivity of any compound.[58]
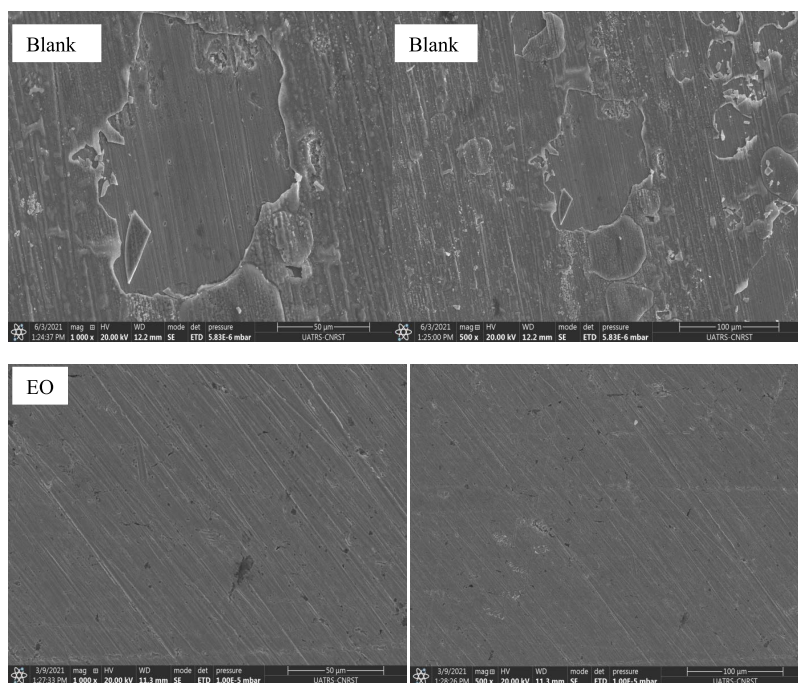


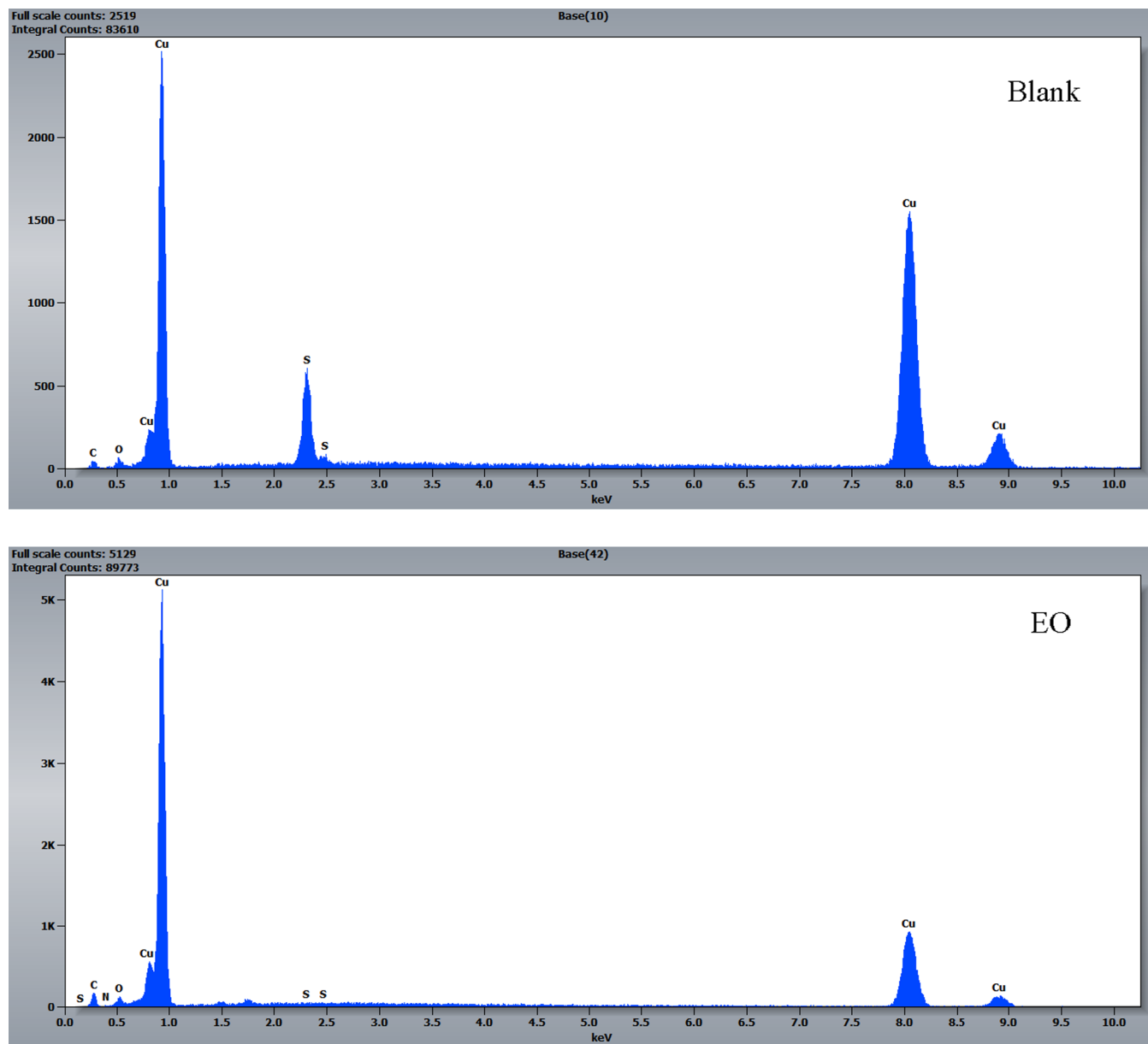**Figure 7.** SEM micrographs of the noninhibited and inhibited Cu metal (after the addition of 2 g L$^{-1}$).

**Figure 8.** EDS spectra of copper substrates submerged in the corrosive acid alone and in a corrosive solution with 2.0 g L$^{-1}$.

**Table 8. Copper Surface Compositions Tested by EDS Analysis**

| element | blank | 2 g/L EO |
|---------|-------|----------|
| C | 4.55 | 6.11 |
| O | 2.00 | 1.96 |
| Cu | 84.07 | 91.51 |
| N | | 0.36 |
| S | 9.39 | 0.05 |

The data reported in Table 9 show that $\alpha$-pinene has a lowest $\Delta E$ value (5.15 eV) than $\delta$-3-carene (5.23 eV), limonene (6.57 eV), and cedral (7.72), suggesting that $\alpha$-pinene could offers relatively higher reactivity toward inhibition performance of copper than the other tested ingredients. The hardness descriptors ($\eta$) given in Table 9 depict the hardness of electron transfer of molecules. It is worth mentioning that the inhibition performance if inhibitor tends to increase with low $\eta$ values. This is also reflecting the high reactivity and inhibition performance

of the $\alpha$-pinene moiety.[59,60] Another important descriptor is the ability of molecules to donate electrons to the Cu surface ($\Delta N_{Cu(111)}$). A high and positive value of $\Delta N$ demonstrates that the great capacity of investigated ingredients to donate e- to the cooper surface, especially, the $\alpha$-pinene molecule. We did not consider the effect of the dipole moments trend $\mu$, on the inhibition performance because there is disagreement on its impact.[60-62]

MC simulations have been used to investigate the interaction between EO ingredient active sites and the copper surface Cu(111).[63] The side view of the equilibrium configurations of $\alpha$-pinene, $\delta$-3-carene, limonene, and cedral adsorbed on the Cu(111) surface is displayed in Figure 12. Also, the different energy descriptors attached to this interaction are listed in Table 10. A visual inspection of output images we can see that the compounds adopt near a parallel orientation to the Cu(111) surface, which ensure a better protection of the Cu surface against aggressive ions such as H$_3$O$^+$ and SO$_4^{2-}$.[56] From Table 10, the negative and high $E_{adsorption}$ values indicate the

**2D**                        **3D**

**Blank**

**EO**
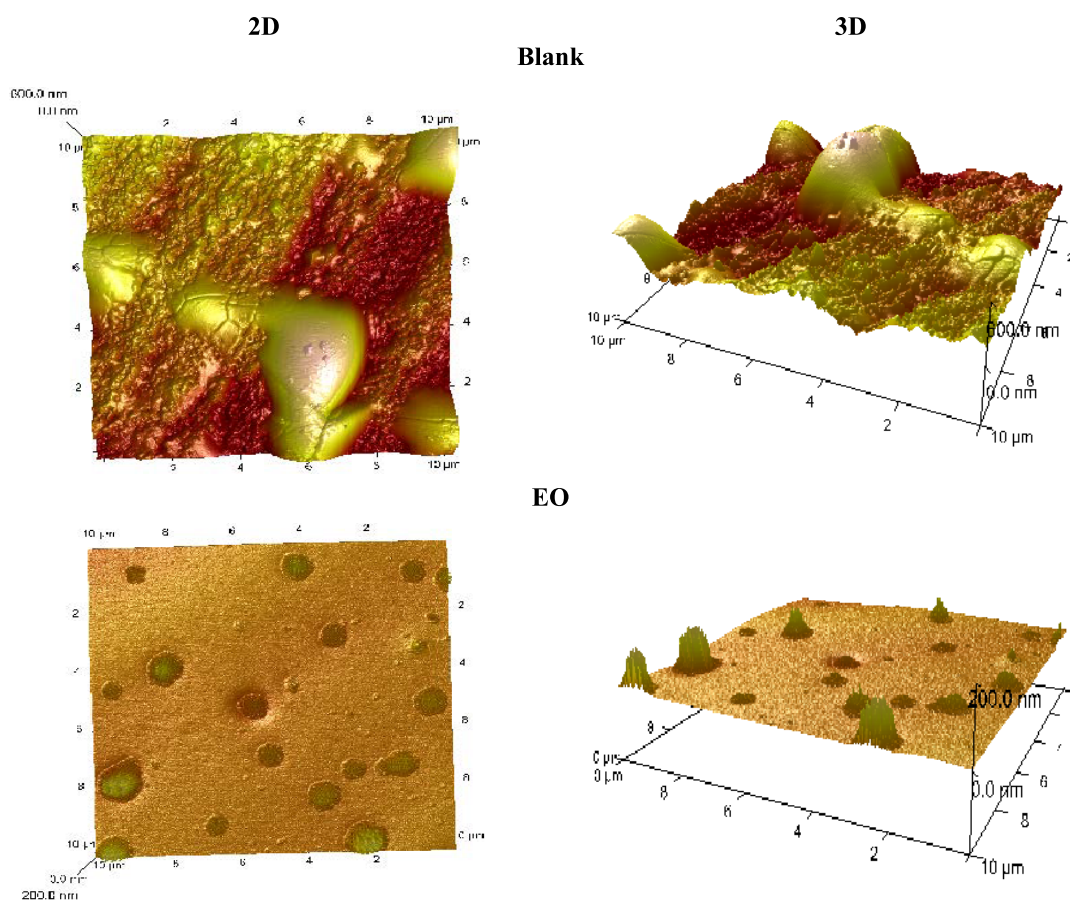
**Average roughness (Ra) measured before and after adding EO inhibitor.**



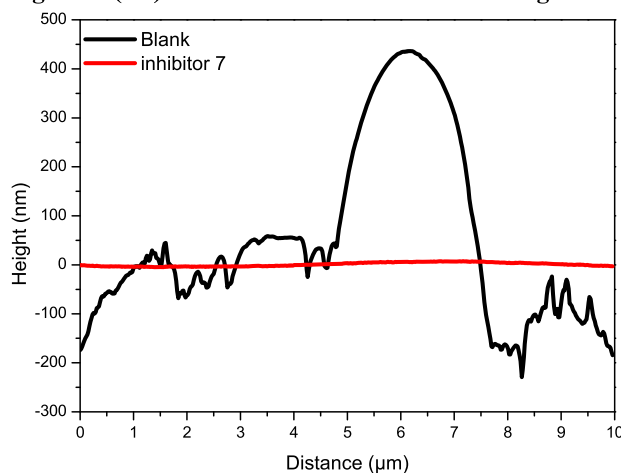**Figure 9.** 2D and 3D AFM images of Cu metal in 0.5 M $H_2SO_4$ solution only and with 2 g/L.

spontaneity and excellent adsorption behavior of $\alpha$-pinene over the Cu surface compared to the other EO ingredients.[64] Therefore, results of this simulation obey the experimental inhibition performance, which suggests that $\alpha$-pinene has the most concentration. In other words, the overall inhibitory effect of the EO can be attributed to $\alpha$-pinene with other components.

The radial distribution function (RDF) was used to calculate the interatomic distance between the atoms of the inhibitor's molecule and copper surface. The probability of finding particle B in the range $r + dr$ around particle A is described by the RDF, $g_{AB}(r)$, which is calculated as follows:

$$g_{AB}(r) = \frac{1}{(\rho_B)_{local}} \times \frac{1}{N_A} \sum_{i \in A}^{N_A} \sum_{i \in B}^{N_B} \frac{\delta(r_{ij} - r)}{4\pi r^2}$$

where $\rho_B$ represents the particle density of B averaged over all shells around particle A.

The determination of interatomic bond lengths is crucial in identifying the type and nature of the formed bonds. Typically, bond lengths falling within the range of 1−3.5 Å are indicative of chemical bonds, whereas peaks exceeding 3.5 Å are associated with physical connections.[65] As shown in Figure 13, the RDF varies as a function of bond lengths ($r$) for the $\alpha$-pinene, $\delta$-3-carene, limonene, and cedral adsorption system on Cu(111).
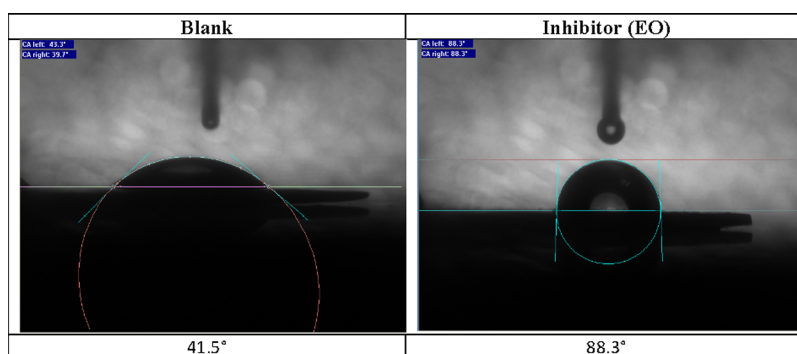
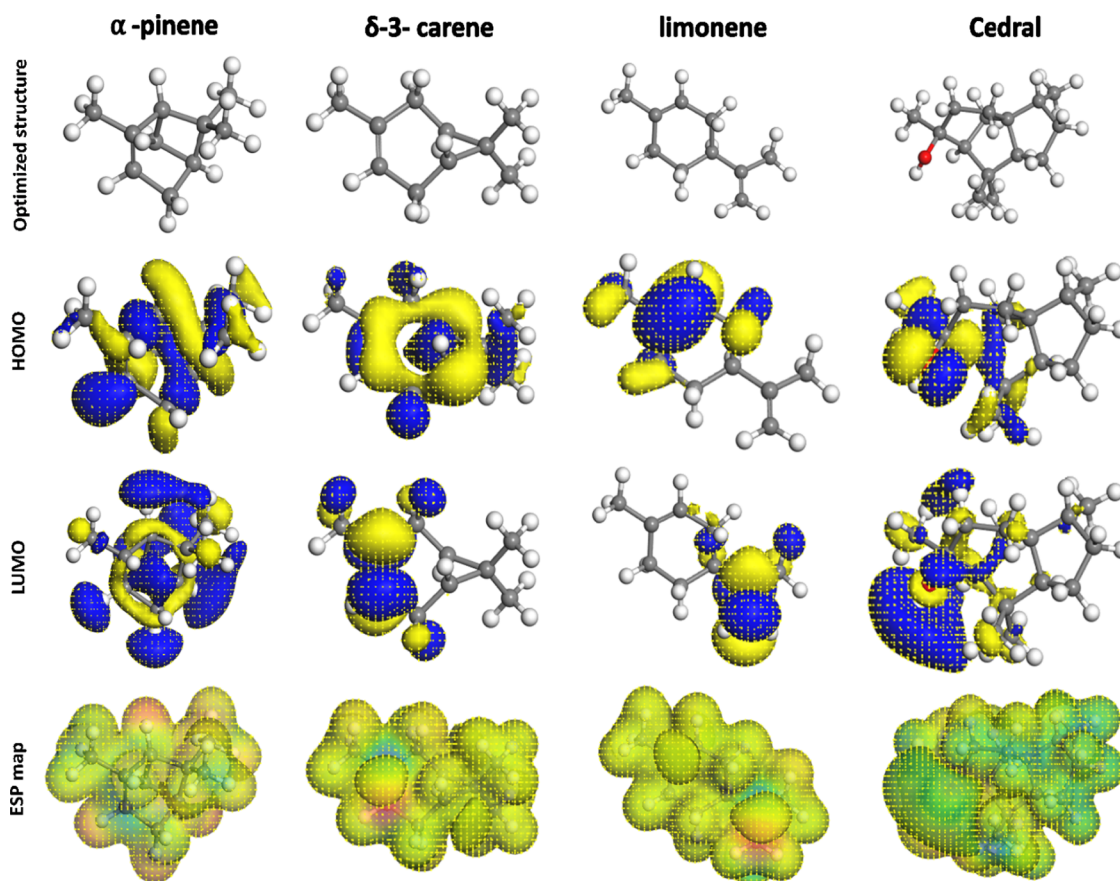**Figure 10.** Contact angle measurement for Cu submerged in 0.5 M $H_2SO_4$ solution only and with 2.0 g $L^{-1}$ for 6 h.



**Figure 11.** Geometry optimized structure, HOMO, and LUMO structures of $\alpha$-pinene, $\delta$-3-carene, limonene, and cedral.

**Table 9. A Variety of Chemical Quantum of Parameters Derived for $\alpha$-Pinene, $\delta$-3-Carene, Limonene, and cedral Compounds Using the DMol3/DND Control**

| compound | $E_{HOMO}$ (eV) | $E_{LUMO}$ (eV) | $\Delta E$ (eV) | $A$ (eV) | $\eta$ (eV) | $\sigma$ (eV) | $\Delta N$ (e) | $\mu$ (Debye) |
|---|---|---|---|---|---|---|---|---|
| $\alpha$-pinene | −5.004 | 0.1480 | 5.1525 | −0.1480 | 2.5762 | 0.3881 | 0.4641 | 0.4036 |
| $\delta$-3-carene | −5.0464 | 0.1799 | 5.2263 | −0.1799 | 2.6131 | 0.3827 | 0.4568 | 0.1634 |
| limonene | −5.3415 | 1.2301 | 6.5716 | −1.2301 | 3.2858 | 0.30433 | 0.4176 | 1.3761 |
| cedral | −5.7507 | 1.9659 | 7.7166 | −1.9659 | 3.8583 | 0.2592 | 0.3794 | 0.0671 |

The results presented in the figure show peak at ∼2.578 Å which suggest that chemical bond formation between the tested inhibitors and the Cu(111) surface is more likely, which aligns with the adsorption isotherm analysis previously discussed.

**3.11. Corrosion Inhibition Mechanism.** The adsorption mechanism of some of the organic constituents present in EO on the copper surface in the acidic environment can be illustrated in

Figure 14. As we can see, the Cu surface rapidly oxidized due to the aggressive acidic environment that makes the metal surface positively charged, which in turn favors the attraction of negatively charged counter sulfate anions resulting in a negative metallic surface. In addition to that, the organic compounds could be protonated in such acidic environment as follows:
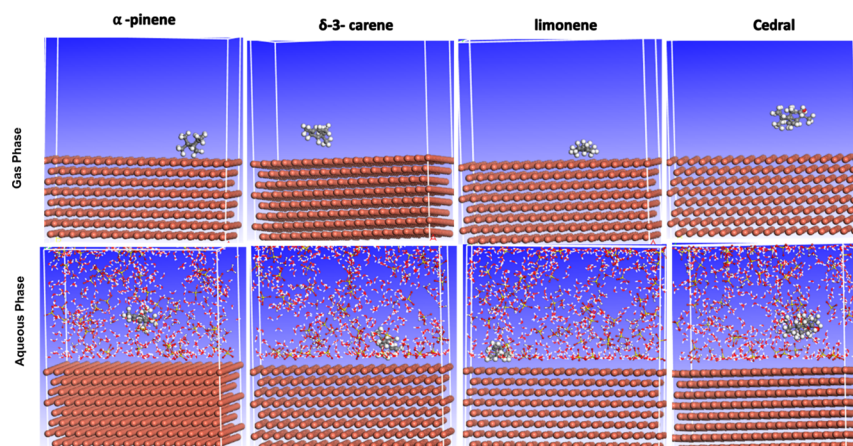
**Figure 12.** Side views for the most stable patterns of α-pinene, δ-3-carene, limonene, and cedral compounds on Cu(111) in the simulated system.

**Table 10. Derived Values of Energy of α-Pinene, δ-3-Carene, Limonene, and Cedral on the Cu(111) Surface in Gas and Aqueous Phases**

| compound | total energy (kJ/mol) | adsorption energy (kcal/mol) | rigid adsorption energy (kcal/mol) | deformation energy (kcal/mol) | inhibitor: ($dE_{ads}$ /dNi) (kcal/mol) | sulfate: ($dE_{ads}$ /dNi) (kcal/mol) | water: ($dE_{ads}$ /dNi) (kcal/mol) |
|---|---|---|---|---|---|---|---|
| | | | | gas-phase | | | |
| α-pinene | −31.85 | −265346.0 | −31.95 | −265314.1 | −265346.0 | | |
| δ-3-carene | 36.06 | −39.40 | −39.33 | −0.07 | −39.40 | | |
| limonene | −65.80 | −45.34 | −46.84 | 1.50 | −45.34 | | |
| cedral | −92.86 | −52.90 | −48.98 | −3.91 | −52.90 | | |
| | | | | solution phase ($500H_2O + 50H_3O^+ + 50SO_4^{2-}$) | | | |
| α-pinene | −25881.22 | −303372.10 | −22227.64 | −281144.50 | −265355.60 | −33.37 | −649.21 |
| δ-3-carene | −26039.78 | −38291.99 | −22192.13 | −16099.85 | −43.76 | −34.49 | −636.84 |
| limonene | −26133.27 | −38289.56 | −22220.13 | −16069.43 | −49.09 | −33.44 | −649.23 |
| cedral | −26089.76 | −38226.54 | −22221.38 | −16005.16 | −68.33 | −28.03 | −648.81 |
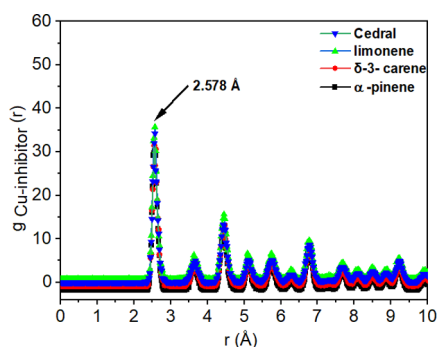


**Figure 13.** RDF plots of different inhibitors on the Cu(111) adsorption system.



**Figure 14.** Schematic illustration of the adsorption mechanism of some of the organic compounds on the surface of copper in a 0.5 M $H_2SO_4$ solution.

$$[Inh] + xH^+ \rightleftharpoons [H_xInh]^{x+}$$

The inhibitor molecules in their protonated state adhere to the negatively charged metal surface due to the attractive electrostatic forces. Furthermore, the lone pair electrons of oxygen atoms, and the π-electrons of the benzene ring, could supply electrons to the vacant d-orbitals of the Cu atoms which leads to the phenomenon of chemisorption.[66] Besides the abovementioned adsorption types, there is a reverse electron's transfer from the d-orbitals of the metal atoms on the surface to the unoccupied molecular orbitals of the inhibitor molecules. This process strengthens the adsorption of the inhibitor molecules on the metal surface. Consequently, it is expected that in an aggr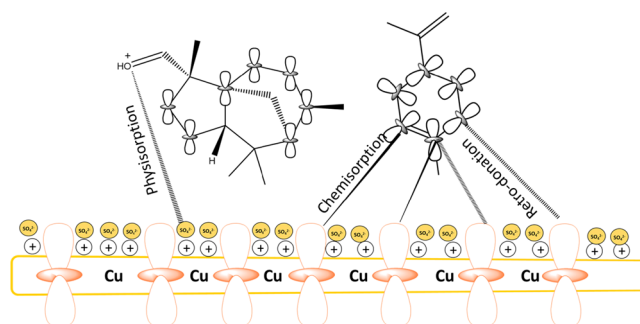essive acidic solution (0.5 M $H_2SO_4$), the adsorption of different inhibitor molecules onto the metal surface of copper will encompass three distinct phenomena: physisorption, chemisorption, and retro-donation.

## 4. CONCLUSIONS

The researchers used both experimental and theoretical approaches to investigate the inhibitive performance and mechanism of EO copper corrosion in a 1 M $H_2SO_4$ solution. Based on their findings, the following conclusions were drawn:

- The results of EIS indicated that at a concentration of 2 g/L, the inhibition efficiency of EO for Cu was over 94% at 298 K. Additionally, the inhibition efficiency increased as the concentration of EO increased. Thus, EO was found

to be a practical and effective mixed-type corrosion inhibitor for Cu in a 0.5 M sulfuric acid solution.

- The Langmuir model revealed that physisorption occurred at the copper/solution interface, with the former playing a leading role. Furthermore, SEM/EDS and AFM microscopic analyses and contact angle measurements confirmed that the formation of a film effectively protected the copper.

- The negative and high adsorption values indicated that $\alpha$-pinene exhibited spontaneous and excellent adsorption behavior over the Cu surface compared to other EO ingredients.

## ■ AUTHOR INFORMATION

### Corresponding Author

Mouhsine Galai − *Advanced Materials and Process Engineering, Faculty of Sciences, Ibn Tofaïl University, 14000 Kenitra, Morocco;* ⓘ orcid.org/0000-0003-3199-9403; Email: galaimouhsine@gmail.com

### Authors

Khadija Dahmani − *Laboratory of Organic, Inorganic Chemistry, Electrochemistry and Environment, Faculty of Sciences, Ibn Tofaïl University, 14000 Kenitra, Morocco*

Adil Ech-Chebab − *Advanced Materials and Process Engineering, Faculty of Sciences, Ibn Tofaïl University, 14000 Kenitra, Morocco*

Nabil Al-Zaqri − *Department of Chemistry, College of Science, King Saud University, Riyadh 11451, Saudi Arabia*

Moussa Ouakki − *Laboratory of Organic, Inorganic Chemistry, Electrochemistry and Environment, Faculty of Sciences and National Higher School of Chemistry (NHSC), Ibn Tofaïl University, 14000 Kenitra, Morocco*

Amr Elgendy − *Egyptian Petroleum Research Institute, 11727 Cairo, Egypt;* ⓘ orcid.org/0000-0001-7442-7865

Rabab Ez-Zriouli − *Laboratory of Agrophysiology, Biotechnology, Environment and Quality, Faculty of sciences, Ibn Tofaïl University, 14000 Kenitra, Morocco*

Seong-Cheol Kim − *School of Chemical Engineering, Yeungnam University, Gyeongsan 38541, Republic of Korea*

Mohamed Ebn Touhami − *Advanced Materials and Process Engineering, Faculty of Sciences, Ibn Tofaïl University, 14000 Kenitra, Morocco*

Mohammed Cherkaoui − *Laboratory of Organic, Inorganic Chemistry, Electrochemistry and Environment, Faculty of Sciences, Ibn Tofaïl University, 14000 Kenitra, Morocco; Department of Chemistry, College of Science, King Saud University, Riyadh 11451, Saudi Arabia*

Complete contact information is available at:
https://pubs.acs.org/10.1021/acsomega.3c00589

### Notes

The authors declare no competing financial interest.

## ■ REFERENCES

(1) Verma, D. K.; Ebenso, E. E.; Quraishi, M. A.; Verma, C. Gravimetric, electrochemical surface and density functional theory study of acetohydroxamic and benzohydroxamic acids as corrosion inhibitors for copper in 1 M HCl. *Results Phys.* **2019**, *13*, No. 102194.

(2) Zhang, J.; Zhang, L.; Tao, G. A novel and high-efficiency inhibitor of 5-(4-methoxyphenyl)-3h-1,2-dithiole-3-thione for copper corrosion inhibition in sulfuric acid at different temperatures. *J. Mol. Liq.* **2018**, *272*, 369−379.

(3) Saha, S. K.; Murmu, M.; Murmu, N. C.; Banerjee, P. Benzothiazolylhydrazine azomethine derivatives for efficient corrosion inhibition of mild steel in acidic environment: Integrated experimental and density functional theory cum molecular dynamics simulation approach. *J. Mol. Liq.* **2022**, *364*, No. 120033.

(4) Singh, A.; Ansari, K. R.; Bedi, P.; Pramanik, T.; Ali, I. H.; Lin, Y.; Banerjee, P.; Zamindar, S. Understanding xanthone derivatives as novel and efficient corrosion inhibitors for P110 steel in acidizing fluid: Experimental and theoretical studies. *J. Phys. Chem. Solids* **2023**, *172*, No. 111064.

(5) Saha, S. K.; Banerjee, P. Introduction of newly synthesized Schiff base molecules as efficient corrosion inhibitors for mild steel in 1 M HCl medium: an experimental, density functional theory and molecular dynamics simulation study. *Mater. Chem. Front.* **2018**, *2*, 1674−1691.

(6) Philippi, F.; Welton, T. Targeted modifications in ionic liquids−from understanding to design. *Phys. Chem. Chem. Phys.* **2021**, *23*, 6993−7021.

(7) Sengupta, S.; Murmu, M.; Mandal, S.; Hirani, H.; Banerjee, P. Competitive corrosion inhibition performance of alkyl/acyl substituted 2-(2-hydroxybenzylideneamino) phenol protecting mild steel used in adverse acidic medium: A dual approach analysis using FMOs/molecular dynamics simulation corroborated experimental findings. *Colloids Surf., A* **2021**, *617*, No. 126314.

(8) Sarkar, S.; Sengupta, S.; Saha, S. K.; Murmu, N. C.; Dutta, S.; Banerjee, P. Quantifying corrosion inhibition on mild steel surface using run length statistics-based texture analysis. *J. Adhes. Sci. Technol.* **2022**, *36*, 2505−2526.

(9) Mandal, S.; Zamindar, S.; Sarkar, S.; Murmu, M.; Guo, L.; Kaya, S.; Hirani, H.; Banerjee, P. Quantum chemical and molecular dynamics simulation approach to investigate adsorption behaviour of organic azo dyes on TiO2 and ZnO surfaces. *J. Adhes. Sci. Technol.* **2023**, *37*, 1649−1665.

(10) Jmiai, A.; El Ibrahimi, B.; Tara, A.; et al. The effect of the two biopolymers "sodium alginate and chitosan" on the inhibition of copper corrosion in 1 M hydrochloric acid. *Mater Today Proc.* **2020**, *22*, 12−15.

(11) Farahati, R.; Behzadi, H.; Mousavi, K. S. M.; Ghaffarinejad, A. Evaluation of corrosion inhibition of 4-(pyridin-3-yl) thiazol-2-amine for copper in HCl by experimental and theoretical studies. *J. Mol. Struct.* **2020**, *1205*, No. 127658.

(12) Dahmani, K.; Galai, M. A.; Elhasnaoui, B.; Temmar, A.; El Hessni, M.; Cherkaoui, M. Corrosion resistance of electrochemical copper coating realized in the presence of essential oils. *Der Pharma Chem.* **2015**, *7*, 566.

(13) El Hamdani, N.; Fdil, R.; Tourabi, M.; Jama, C.; Bentiss, F. Alkaloids extract of Retama monosperma (L.) Boiss. seeds used as novel eco-friendly inhibitor for carbon steel corrosion in 1 M HCl solution: Electrochemical and surface studies. *Appl. Surf. Sci.* **2015**, *357*, 1294−1305.

(14) Galai, M.; Rbaa, M.; Ouakki, M.; et al. Effect of alkyl group position on adsorption behavior and corrosion inhibition of new naphthol based on 8-hydroxyquinoline: Electrochemical, surface, quantum calculations and dynamic simulations. *J. Mol. Liq.* **2021**, *335*, No. 116552.

(15) Farahati, R.; Ghaffarinejad, A.; Mousavi-Khoshdel, S. M.; Rezania, J.; Behzadi, H.; Shockravi, A. Synthesis and potential applications of some thiazoles as corrosion inhibitor of copper in 1 M HCl: Experimental and theoretical studies. *Prog. Org. Coat.* **2019**, *132*, 417−428.

(16) Tan, B.; Zhang, S.; Qiang, Y.; et al. Experimental and theoretical studies on the inhibition properties of three diphenyl disulfide derivatives on copper corrosion in acid medium. *J. Mol. Liq.* **2020**, *298*, No. 111975.

(17) Behpour, M.; et al. Green approach for corrosion inhibition of mild steel in hydrochloric acid solution by Punica granatum peel extract. *J. Ind. Eng. Chem.* **2014**, *20*, 103−112.

(18) Al-Mobarak, N. A.; et al. Green approach for corrosion inhibition of mild steel in HCl solution by Allium sativum extract. *J. Mol. Liq.* **2015**, *210*, 295−303.

(19) Kurniawan, T.; et al. The use of Zingiber officinale extract as a green corrosion inhibitor for mild steel in 1 M HCl solution. *J. Appl. Electrochem.* **2019**, *49*, 877−890.

(20) Singh, S.; et al. Emblica officinalis extract as a green corrosion inhibitor for mild steel in acidic medium. *J. Mol. Liq.* **2018**, *268*, 74−87.

(21) Selvi, J. A.; et al. Green approach for corrosion control of mild steel in HCl medium using Azadirachta indica leaves extract. *J. Mol. Liq.* **2016**, *219*, 66−76.

(22) Balusamy, T.; et al. Syzygium aromaticum extract as a green corrosion inhibitor for mild steel in hydrochloric acid solution. *J. Ind. Eng. Chem.* **2014**, *20*, 376−385.

(23) Dahmani, K.; Galai, M.; Ech-chebab, A.; Ouakki, M.; Kadiri, L.; Elgendy, A.; Ez-Zriouli, R.; Cherkaoui, M. Pistacia lentiscus extract as a green inhibitor for copper corrosion in 0.5 M of H2SO4: electrochemical characterization and theoretical investigations. *J. Appl. Electrochem.* **2022**, *52*, 1629−1646.

(24) Ouakki, M.; Galai, M.; Benzekri, Z.; Aribou, Z.; Ech-chihbi, E.; Guo; Dahmani; Nouneh; Briche; Boukhris; Cherkaoui, M. A detailed investigation on the corrosion inhibition effect of by newly synthesized pyran derivative on mild steel in 1 . 0 M HCl : Experimental , surface morphological ( SEM-EDS , DRX & AFM ) and computational analysis (DFT & MD simulation). *J. Mol. Liq.* **2021**, *344*, No. 117777.

(25) Lazrak, J.; El Assiri, E. H.; Arrousse, N.; et al. Origanum compactum essential oil as a green inhibitor for mild steel in 1 M hydrochloric acid solution: Experimental and Monte Carlo simulation studies. *Mater Today Proc.* **2021**, *45*, 7486−7493.

(26) Elgendy, A.; Elkholy, A. E.; El Basiony, N. M.; Migahed, M. A. Monte Carlo simulation for the antiscaling performance of Gemini ionic liquids. *J. Mol. Liq.* **2019**, *285*, 408−415.

(27) Sadeghi, E. R.; Amirnasr, M.; Meghdadi, S.; Talebian, M.; Farrokhpour, H.; Raeissi, K. Carboxamide derivatives as new corrosion inhibitors for mild steel protection in hydrochloric acid solution. *Corros. Sci.* **2019**, *151*, 190−197.

(28) Coelho, L. B.; Mouanga, M.; Druart, M. E.; Recloux, I.; Cossement, D.; Olivier, M. G. A SVET study of the inhibitive effects of benzotriazole and cerium chloride solely and combined on an aluminium/copper galvanic coupling model. *Corros. Sci.* **2016**, *110*, 143−156.

(29) Feng, L.; Zhang, S.; Qiang, Y.; et al. Experimental and theoretical investigation of thiazolyl blue as a corrosion inhibitor for copper in neutral sodium chloride solution. *Materials* **2018**, *11*, 1042.

(30) Jmiai, A.; Tara, A.; El Issami, S.; Hilali, M.; Jbara, O.; Bazzi, L. A new trend in corrosion protection of copper in acidic medium by using Jujube shell extract as an effective green and environmentally safe corrosion inhibitor: Experimental, quantum chemistry approach and Monte Carlo simulation study. *J. Mol. Liq.* **2021**, *322*, No. 114509.

(31) Fawzy, A.; Farghaly, T. A.; Al Bahir, A. A.; Hameed, A. M.; Alharbi, A.; El-ossaily, Y. A. Investigation of three synthesized propane bis-oxoindoline derivatives as inhibitors for the corrosion of mild steel in sulfuric acid solutions. *J. Mol. Struct.* **2021**, *1223*, No. 129318.

(32) Lu, Y.; Zhou, L.; Tan, B.; et al. Two common antihistamine drugs as high-efficiency corrosion inhibitors for copper in 0.5M H2SO4. *J. Taiwan Inst. Chem. Eng.* **2021**, *123*, 11−20.

(33) Qiang, Y.; Zhang, S.; Yan, S.; Zou, X.; Chen, S. Three indazole derivatives as corrosion inhibitors of copper in a neutral chloride solution. *Corros. Sci.* **2017**, *126*, 295−304.

(34) Khrifou, R.; Touir, R.; Koulou, A.; et al. The influence of low concentration of 2-(5-methyl-2-nitro-1H-imidazol-1-yl)ethyl benzoate on corrosion brass in 0.5 M H2SO4 solution. *Surf. Interfaces* **2021**, *24*, No. 101088.

(35) Qiang, Y.; Zhang, S.; Wang, L. Understanding the adsorption and anticorrosive mechanism of DNA inhibitor for copper in sulfuric acid. *Appl. Surf. Sci.* **2019**, *492*, 228−238.

(36) Zhang, Y.; Zhang, S.; Tan, B.; Guo, L.; Li, H. Solvothermal synthesis of functionalized carbon dots from amino acid as an eco-friendly corrosion inhibitor for copper in sulfuric acid solution. *J. Colloid Interface Sci.* **2021**, *604*, 1−14.

(37) Qiang, Y.; Guo, L.; Li, H.; Lan, X. Fabrication of environmentally friendly Losartan potassium film for corrosion inhibition of mild steel in HCl medium. *Chem. Eng. J.* **2021**, *406*, No. 126863.

(38) Qiang, Y.; Li, H.; Lan, X. Self-assembling anchored film basing on two tetrazole derivatives for application to protect copper in sulfuric acid environment. *J. Mater. Sci. Technol.* **2020**, *52*, 63−71.

(39) Tasic, Z. Z.; Antonijevic, M. M.; Petrovic Mihajlovic, M. B.; Radovanovic, M. B. The influence of synergistic effects of 5-methyl-1H-benzotriazole and potassium sorbate as well as 5-methyl-1H-benzotriazole and gelatin on the copper corrosion in sulphuric acid solution. *J. Mol. Liq.* **2016**, *219*, 463−473.

(40) Tan, B.; Zhang, S.; Qiang, Y.; et al. Investigation of the inhibition effect of Montelukast Sodium on the copper corrosion in 0.5 mol/L H2SO4. *J. Mol. Liq.* **2017**, *248*, 902−910.

(41) Khaled, K. F. Adsorption and inhibitive properties of a new synthesized guanidine derivative on corrosion of copper in 0.5 M H 2 SO 4. *Appl. Surf. Sci.* **2008**, *255*, 1811−1818.

(42) Moretti, G.; Guidi, F. Tryptophan as copper corrosion inhibitor in 0.5 M aerated sulfuric acid. *Corros. Sci.* **2002**, *44*, 1995−2011.

(43) Chen, S.; Chen, S.; Zhu, B.; Huang, C.; Li, W. Magnolia grandi fl ora leaves extract as a novel environmentally friendly inhibitor for Q235 steel corrosion in 1 M HCl : Combining experimental and theoretical researches. *J. Mol. Liq.* **2020**, *311*, No. 113312.

(44) Ech-chebab, A.; Missioui, M.; Guo, L.; El Khouja, O.; Lachhab, R.; Kharbouch, O.; Galai, M.; Ouakki, M.; Ejbouh, A.; Dahmani, K.; Dkhireche, N.; Ebn Touhami, M. Evaluation of quinoxaline-2 ( 1H ) -one , derivatives as corrosion inhibitors for mild steel in 1. 0 M acidic media : Electrochemistry, quantum calculations, dynamic simulations and surface analysis. **2022**, *809* (16), 140156, .

(45) Gao, L.; Peng, S.; Huang, X.; Gong, Z. A combined experimental and theoretical study of papain as a biological eco-friendly inhibitor for copper corrosion in H2SO4 medium. *Appl. Surf. Sci.* **2020**, *511*, No. 145446.

(46) Chung, I. M.; Malathy, R.; Priyadharshini, R.; Hemapriya, V.; Kim, S. H.; Prabakaran, M. Inhibition of mild steel corrosion using Magnolia kobus extract in sulphuric acid medium. *Mater Today Commun.* **2020**, *25*, No. 101687.

(47) Xu, S.; Luo, Z.; Zhang, J.; Tan, B.; Zhang, S.; Li, W. Study on corrosion inhibition performance of 1-dodecyl-3-methyl-1 h-imidazolium nitrate on Cu in the sulfuric acid environment. *J. Mol. Liq.* **2021**, *340*, No. 117189.

(48) Benhiba, F.; Sebbar, N. K.; Bourazmi, H.; et al. Corrosion inhibition performance of 4-(prop-2-ynyl)- [1,4]-benzothiazin-3-one against mild steel in 1 M HCl solution: Experimental and theoretical studies. *Int. J. Hydrogen Energy* **2021**, *46*, 25800−25818.

(49) Xu, Y.; Zhang, S.; Li, W.; et al. Experimental and theoretical investigations of some pyrazolo-pyrimidine derivatives as corrosion inhibitors on copper in sulfuric acid solution. *Appl. Surf. Sci.* **2018**, *459*, 612−620.

(50) Shi, Y.; Fu, Y.; Xu, S.; et al. Strengthened adsorption and corrosion inhibition of new single imidazole-type ionic liquid molecules to copper surface in sulfuric acid solution by molecular aggregation. *J. Mol. Liq.* **2021**, *338*, No. 116675.

(51) Tan, B.; Zhang, S.; Cao, X.; et al. Insight into the anti-corrosion performance of two food flavors as eco-friendly and ultra-high performance inhibitors for copper in sulfuric acid medium. *J. Colloid Interface Sci.* **2022**, *609*, 838−851.

(52) Galai, M.; Rbaa, M.; Ouakki, M.; et al. Functionalization effect on the corrosion inhibition of novel eco-friendly compounds based on 8-hydroxyquinoline derivatives: Experimental, theoretical and surface treatment. *Chem. Phys. Lett.* **2021**, *776*, No. 138700.

(53) Li, W.; Zhang, Z.; Zhai, Y.; Ruan, L.; Zhang, W.; Wu, L. Electrochemical and computational studies of proline and captopril as corrosion inhibitors on carbon steel in a phase change material solution. *Int. J. Electrochem. Sci.* **2020**, *15*, 722−739.

(54) Alibakhshi, E.; Ramezanzadeh, M.; Bahlakeh, G.; Ramezanzadeh, B.; Mahdavian, M.; Motamedi, M. Glycyrrhiza glabra leaves extract as a green corrosion inhibitor for mild steel in 1 M hydrochloric acid solution : Experimental , molecular dynamics, Monte Carlo and quantum mechanics study. *J. Mol. Liq.* **2018**, *255*, 185−198.

(55) Ouakki, M.; Galai, M.; Aribou, Z.; Benzekri, Z.; Dahmani, K.; Ech-chihbi, E.; Abousalem, A. S.; Boukhris, S.; Cherkaoui, M. Detailed experimental and computational explorations of pyran derivatives as corrosion inhibitors for mild steel in 1.0 M HCl: Electrochemical/ surface studies, DFT modeling, and MC simulation. *J. Mol. Struct.* **2022**, *1261*, No. 132784.

(56) Barbouchi, M.; Benzidia, B.; Aouidate, A.; Ghaleb, A.; El Idrissi, M.; Choukrad, M. Theoretical modeling and experimental studies of Terebinth extracts as green corrosion inhibitor for iron in 3% NaCl medium. *J. King Saud. Univ. Sci.* **2020**, *32*, 2995−3004.

(57) Oubaaqa, M.; Ouakki, M.; Rbaa, M.; Benhiba, F.; Galai, M.; Idouhli, R.; Maatallah, M.; Jarid, A.; Warad, I.; Lakhrissi, B. *J. Phys. Chem. Solids* **2022**, *169*, No. 110866.

(58) Qiang, Y.; Zhang, S.; Guo, L.; Zheng, X.; Xiang, B.; Chen, S. Experimental and theoretical studies of four allyl imidazolium-based ionic liquids as green inhibitors for copper corrosion in sulfuric acid. *Corros. Sci.* **2017**, *119*, 68−78.

(59) Nady, H.; Elgendy, A.; Arafa, W. A. A.; Gad, E. S. Insight into the inhibition performance of thiosemicarbazones as efficient inhibitors for copper in acidic environment: Combined experimental and computational investigations. *Colloids Surf., A* **2022**, *647*, No. 129208.

(60) Abbas, M. A.; Eid, A. M.; Abdou, M. M.; Elgendy, A.; El-Saeed, R. A.; Zaki, E. G. Multifunctional Aspects of the Synthesized Pyrazoline Derivatives for AP1 5L X60 Steel Protection against MIC and Acidization: Electrochemical, in Silico, and SRB Insights. *ACS Omega* **2021**, *6*, 8894−8907.

(61) Dahmani, K.; Galai, M.; Ouakki, M.; Elgendy, A.; Ez-Zriouli, R.; Lachhab, R.; Briche, S.; Cherkaoui, M. Corrosion inhibition of copper in sulfuric acid via environmentally friendly inhibitor (Myrtus Communis): Combining experimental and theoretical methods. *J. Mol. Liq.* **2022**, *347*, No. 117982.

(62) Qiang, Y.; Zhi, H.; Guo, L.; Fu, A.; Xiang, T.; Jin, Y. Experimental and molecular modeling studies of multi-active tetrazole derivative bearing sulfur linker for protecting steel from corrosion. *J. Mol. Liq.* **2022**, *351*, No. 118638.

(63) Rbaa, M.; Dohare, P.; Berisha, A.; et al. New Epoxy sugar based glucose derivatives as eco friendly corrosion inhibitors for the carbon steel in 1.0 M HCl: Experimental and theoretical investigations. *J. Alloys Compd.* **2020**, *833*, No. 154949.

(64) Oubaaqa, M.; Ouakki, M.; Rbaa, M.; et al. Insight into the corrosion inhibition of new amino-acids as efficient inhibitors for mild steel in HCl solution: Experimental studies and theoretical calculations. *J. Mol. Liq.* **2021**, *334*, No. 116520.

(65) Benhiba, F.; Serrar, H.; Hsissou, R.; Guenbour, A.; Bellaouchou, A.; Tabyaoui, M.; Zarrouk, A. Tetrahydropyrimido-Triazepine derivatives as anti-corrosion additives for acid corrosion: Chemical, electrochemical, surface and theoretical studies. *Chem. Phys. Lett.* **2020**, 743.

(66) Basiony, N. E.; Elgendy, A.; Nady, H.; Migahed, M. A.; Zaki, E. G. Adsorption characteristics and inhibition effect of two Schiff base compounds on corrosion of mild steel in 0.5 M HCl solution: experimental, DFT studies, and Monte Carlo simulation. *RSC Adv.* **2019**, *9*, 10473−10485.